OBSERVATIONS OF WINTER STORMS WITH 2-D VIDEO DISDROMETER AND POLARIMETRIC RADAR

Kyoko Ikeda*, Edward A. Brandes, and Guifu Zhang
National Center for Atmospheric Research, Boulder, Colorado

1. Introduction

The Winter Icing and Storms Project 2004 (WISP04) was conducted from February to April 2004 in north central Colorado. Program objectives were to evaluate remote sensing techniques for icing detection and to quantify winter precipitation in support of airport deicing operations. Measurements from a S-band dual-polarization radar and a two-dimensional video disdrometer are being used to develop radar-based algorithms to discriminate between rain and snow, quantify winter precipitation, and improve parameterization of winter precipitation in numerical forecast models. Winter precipitation often includes liquid, mixed-phase, and frozen hydrometeors and evolves continuously throughout the event. An ability to match radar-measured and disdrometer-based radar parameters is essential when developing radar-based algorithms for winter precipitation. Disdrometers provide important information regarding hydrometeor size, terminal velocity, shape, and number concentration at high temporal resolution. As a first step in this ambitious project, we verify that the radar detects subtle changes in the character of winter precipitation.

Here radar reflectivity factor (reflectivity or Z_H, hereafter) and differential reflectivity (Z_{DR}) are calculated from disdrometer data collected on 5 March 2004, an event in which precipitation changed from rain to snow. The retrieval is based on scattering amplitudes of raindrops and snow computed with the T-matrix method. The scattering matrix during the transition and snow phases was allowed to vary according to an empirical relation between particle size and bulk snow density developed from disdrometer observations. Reflectivity and differential reflectivity calculations based on disdrometer observations show good agreement with the radar measurements.

The dataset and a brief description of the disdrometer are given in section 2. Section 3 discusses the retrieval method for reflectivity and differential reflectivity followed by a comparison of the retrievals with the radar measurements (Section 4). A summary and concluding remarks are given in section 5.

2. Data

The radar data were collected with NCAR's S-band dual-polarization radar located at Marshall, Colorado. Scan strategies included sector scans at 0.5 and 1.5° elevations and range-height indicator (RHI) scans over a 2-D video disdrometer placed at a range of 19 km and an azimuth angle of 42° from the radar.

The disdrometer consists of two line-scan cameras providing front and side views of hydrometers falling into the instrument. Each camera has a single line of 700 photo-detectors positioned opposite a light source. Hydrometeors falling through the 10 cm by 10 cm measuring area block the light source, shadowing some photo-detectors at a resolution of 0.15 mm. The number of blocked photo-detectors is recorded for each camera at a frequency of 34.1 kHz. The sampling creates image projection slices of the hydrometeors.

Information provided on individual hydrometeors includes silhouette images, height and width information from each camera, and the particle terminal velocity. Particle terminal velocity is computed from the vertical distance between the two camera planes and the time the hydrometeor takes to break each plane. Raindrop axis ratio, canting angle, and horizontal velocity can also be obtained with the instrument. The disdrometer is equipped with temperature and wind sensors. A detailed description is found in Kruger and Krajewski (2002). Field notes from a crystal observer at the disdrometer site supplement the disdrometer data. Observations of crystal type, size, degree of riming, and amount of aggregation were made every 15 minutes.

3. Modeling considerations

Radar reflectivity (in mm^6 m^{-3}) at horizontal (H) and vertical (V) polarization can be computed from

$$Z_{H,V} = \frac{4\lambda^4}{\pi^4 \left|K_w\right|^2} \sum_{i=1}^{M} N(D_i) \left|f_{H,V}\right|^2 \Delta D \qquad (1)$$

where λ is the radar wavelength, K_w is the dielectric factor of water, $N(D_i)$ is the size distribution for the ith size category having an equivalent diameter (mm) between D_i and $D_i + \Delta D$, M is the total number of size categories, and $\left|f_{H,V}\right|$ is the scattering amplitude at horizontal and vertical polarization (see Zhang et al. 2001). In this study, the disdrometer data were quantitized into size categories of 0.2 mm over the range of 0.1-20.1 mm for snow and 0.1-8.1 mm for rain. Reflectivity is expressed in dBZ ($10 \times \log_{10} Z_H$).

---

* *Corresponding author address:* Kyoko Ikeda, National Center for Atmospheric Research, P.O. Box 3000, Boulder, CO 80307
E-mail: kyoko@ncar.ucar.edu

The differential reflectivity (Z_{DR} in dB) is defined as

$$Z_{DR} = 10 \times \log_{10}(Z_H / Z_V) . \qquad (2)$$

Z_{DR} is sensitive to particle bulk density and canting angle and can be interpreted as the reflectivity-weighted mean axis ratio of the illuminated hydrometeors. The Z_{DR} values were corrected for system bias (−0.08 dB). The bias was determined from radar data that was collected by rotating the antenna while pointing vertically in light rain. In theory, raindrops should produce a Z_{DR} value of 0 dB in the mean when viewed from below.

The scattering amplitude is computed with the T-matrix method (Barber and Yeh 1975). Input parameters include the dielectric constant, particle shape (e.g., axis ratio), and the temperature. For rain these parameters follow Zhang et al. (2001).

Properties of snow are complex. Aspect ratios and bulk densities continuously change throughout storm evolution making computations of the scattering amplitudes less straight forward. In this study, the particles were assumed to be oblate spheroids having a fixed axis ratio (vertical divided by horizontal) of 0.7 and with their major axis along the horizontal.

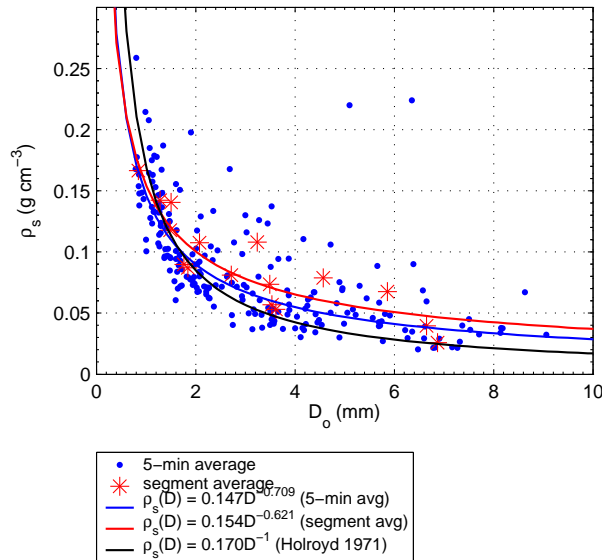The effective dielectric constant (Ishimaru 1991) was derived from disdrometer data collected at Marshall prior to the WISP04 field program. Using measurements of precipitation volume from the disdrometer and mass from precipitation gauges, snow bulk density was computed. All instruments were located inside wind shields. The relation between the median equivolumetric diameter and bulk density from 16 time segments that were selected from nine snow events for which ambient winds were less than 1 m s^{-1} is shown in Fig. 1. Time segments ranged between 30 minutes and 2 hours in duration and were chosen based on the steadiness of particle concentrations and similarities in hydrometeor characteristics (e.g., dominated or not dominated by aggregates). Data points are from particle size distributions (PSD) averaged over 5 minutes (dots) and over each time segment (asterisks). Power-law relations fitted to the 5-minute and the segment PSDs are overlaid. The dataset contains both rimed and unrimed snow. Nevertheless, the data generally follow the inverse relation between size and density found by Holroyd (1971) for unrimed snowflakes. For this study, we use an effective dielectric constant based on the power-law relation corresponding to the 5-minute PSDs. In a sense, the computed scattering amplitude allows for a variation in bulk density that is anticipated to occur with storm evolution. This approach is similar to that taken by Ryzhkov et al. (1998) who proposed a method to compute cloud ice water content using a relation between particle bulk density and radar cross sections.

4. Observations: 5 March 2004

Precipitation on 5 March 2004 was dominated by an intense 500 mb trough across the western United States and an associated surface low pressure system over central Oklahoma. Low-level winds from the east-northeast and northeast behind the low pressure center created a favorable condition for a upslope stratiform precipitation in the WIPS04 domain. Winds above 3 km MSL, i.e., above the upslope layer, were mostly westerly or southwesterly. An abrupt decrease in temperature from 5.5°C to 0.5°C occurred over a 15-minute period at approximately 0100 UTC. The surface temperature changed only slightly afterward remaining between 0.5 and −0.5°C. The temperature at cloud top (5 km MSL) was −15°C.

a. Precipitation

Most of the precipitation fell between 0000 and 0500 UTC. Table 1 summarizes the hydrometeor types noted by the crystal observer. Early precipitation was light rain (Period A). The surface layer moistened and cooled rapidly as the rain rate increased. A rain-to-snow transition (Period B) occurred with the temperature decrease at 0100 UTC. The field notes indicate ice pellets were mixed with raindrops (Fig. 2). The smaller terminal velocities of ice pellets, compared with raindrops, are clearly depicted in the disdrometer data (Fig. 3, Period B). [Terminal velocity relations for raindrops, graupel and aggregates are plotted as a

Figure 1: Relation between snow bulk density (ρ_s) and median volume diameter (D_o) for selected snow events between February 2002 and February 2004. Dots are for PSDs and bulk densities averaged over 5 minutes. Asterisks represent averaged values over selected time segments of the snow events. The blue (red) line is a power-law relation derived for the 5-minute (segment) averages. The black line is an inverse relation of bulk density and diameter for unrimed snow aggregates from Holroyd (1971).

Table 1: Summary of crystal observations taken at the disdrometer site. Crystal types are listed from most to least dominant. Typical aggregate sizes (mm), percentage of total particles identified as aggregates, and degree of riming (none, light, moderate, heavy) are noted. Temperature ranges are from a sensor mounted on the disdrometer.

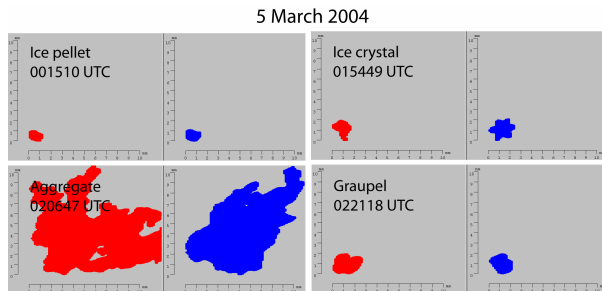|	Time (UTC)	Crystals	Aggregates	Temperature (^{o}C)
A	0000-0100	Rain	—	5.5-7
B	0100-0120	Rain mixed with ice pellets	none	0.5-5.5
C	0120-0145	ice pellets	3-8 mm 30 % light	0.5
D	0145-0220	dendrites, plates, stellars	3-10 mm 40 % light to mod.	0.1
E	0220-0400	irregular snow, lump graupel	2-5 mm 5-20 % light	−0.5-0.1

5 March 2004

Figure 2: Sample hydrometeor images from Period B (ice pellet), Period D (ice crystal and aggregate), and Period E (graupel) from the disdrometer. Red and blue images are the front and side views, respectively. The width and height scales are in mm.

reference.] A small number of large aggregates also existed at this time which caused an increase in the particle median volume diameter (Fig. 4). The mixed-phase precipitation period ended by 0120 UTC.

Later (0120-0145 UTC; Period C), observed precipitation consisted mostly of ice pellets and some small aggregates. Beginning at 0145 UTC (Period D), 1-3 mm plate-like crystals (plates and dendrites) became noticeable, and the number of large aggregates increased significantly. (Figs. 2 and 3, Period D). The observed terminal velocities show a weak relation with aggregate size and follow the unrimed aggregate relation from Locatelli and Hobbs (1974).
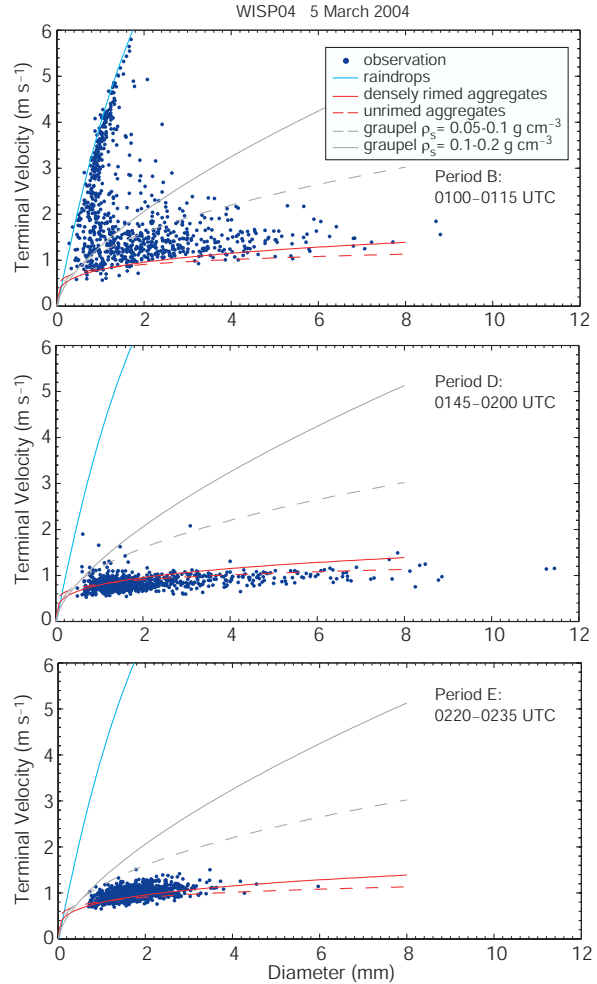

Figure 3: Particle terminal velocity versus diameter for time segments in Period B (top), Period D (middle), and Period E (bottom). Hydrometeor observations during these time periods are indicated in Table 1. Data points represent 1-second volume weighted terminal velocities at sea level. The terminal velocity relation for rain is from Brandes et al. (2002). The relations for graupel and snow aggregates are from Locatelli and Hobbs (1974).

At ~0220 UTC, another change in particle habit occurred (Period E). Hydrometeors were identified as small lump graupel and irregular snow pellets (Figs. 2 and 4). The field notes indicate much less aggregation at this time. The terminal velocity appears to have a slightly stronger size-dependency compared with the previous period (Fig. 3, Period E). The median volume diameter decreased significantly between heavy aggregation during Period D (D_o = 6 mm) and the subsequent graupel/snow pellet Period E ($D_o \leq$ 3 mm). This change would correspond to an estimated bulk density increase of 0.05 g cm^{-3} (Fig. 1).

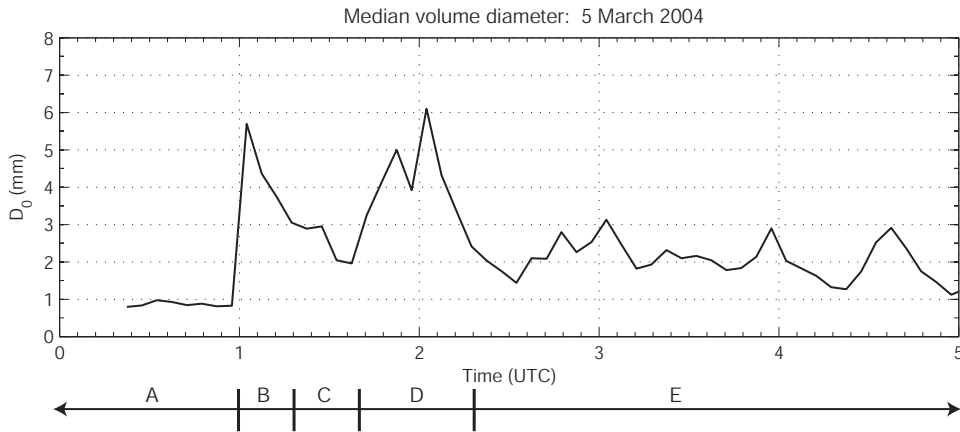b. Comparison of the measured and calculated Z_H and Z_{DR}

Figure 4: Time history of median equivolumetric diameters (D₀) from 5-minute PSDs.
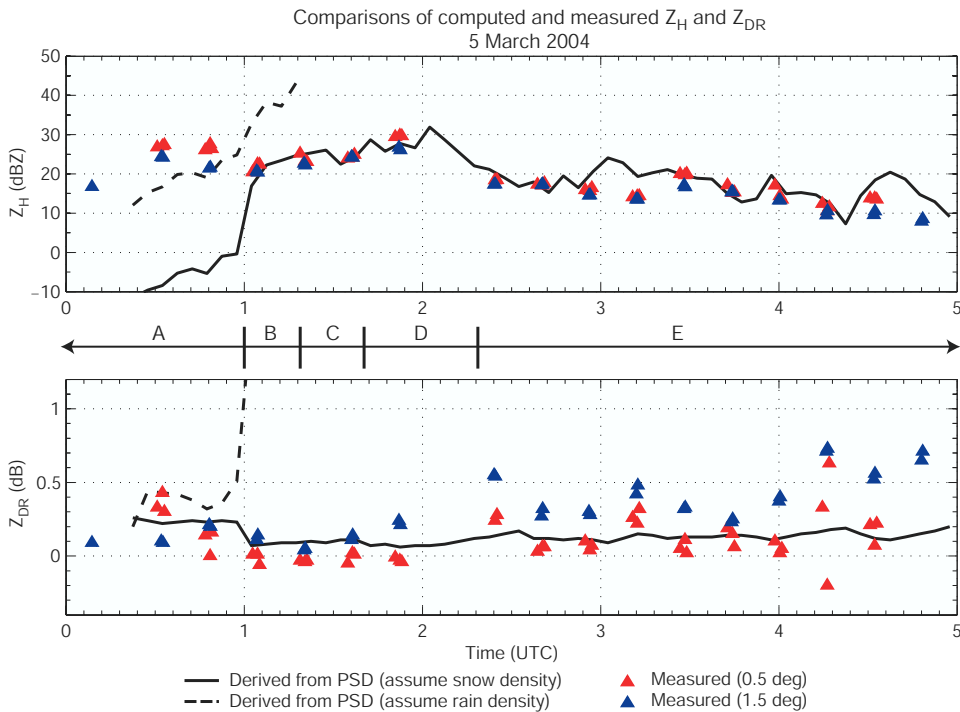

Figure 5: Time histories of measured and retrieved Z_H (top) and Z_{DR} (bottom). Retrievals (solid and dashed lines) are based on 5-minute PSDs. Radar measurements (triangles) are averaged over 1-km in the horizontal at the disdrometer site.

Fig. 5 shows time histories of measured and derived Z_H and Z_{DR}. The radar measurements are averaged over 1 km in the horizontal at the disdrometer site. [The 0.5 and 1.5° elevation radar beams were about 190 and 520 m above the disdrometer, respectively.] Cross sections of Z_H and Z_{DR} were uniform in the horizontal; thus, the computations do not take in account particle trajectories.

The Z_H retrievals with the disdrometer data in Period A are slightly less than the radar measurements.

The Z_H cross sections in the early rain stage show an elevated layer of maximum reflectivity at ~3 km. Evaporation at low levels may also account for the offset between the estimated and measured values. When Z_H is computed assuming that all particles are snow in the rain period (Period A), the retrievals are significantly less than the measurements, reflecting the dependency of Z_H on the hydrometeor dielectric constant.

Agreement between the measured and derived Z_H are excellent during the snow period (after 0100

UTC). Well-matched retrievals in Period B, when using the snow scattering amplitude, probably come from the fact that return signals from large, low density aggregates dominated over the returns from the smaller raindrops and ice pellets. An overall reduction in the particle size and an associated decrease in snowfall rate (Period D and Period E) coincide with a Z_H reduction of 10 dBZ or more.

Similarly, Z_{DR} calculations and measurements for the respective rain and snow phases show good agreement. As with Z_H, Z_{DR} retrievals based on raindrop scattering amplitudes greatly exceed the measurements during the rain-snow transition period. Correspondence for the snow period is attributable in large part to accounting for particle density changes. Small Z_{DR} is associated with low density aggregates in Period B through Period D. The measured and retrieved Z_{DR} values slightly increased when the number of aggregates significantly decreased and small graupel and snow pellets with higher density became dominant (Period E). This Z_{DR} increase was not observed if the bulk density was fixed at a constant value (not shown). During Period E, the measured Z_{DR} decreases toward ground (compare values at 0.5 and 1.5^o elevations). This suggests that particles were more pristine at higher elevations at this stage and that riming and/or aggregation was taking place between the two scan levels causing the particles to become less oblate in the mean as they fell.

5. Summary and concluding remarks

Radar reflectivity and differential reflectivity were computed from disdrometer data and were compared to radar measurements. The scattering amplitudes for snow particles were derived by exploiting an empirical relationship between particle size and snow bulk density. Overall, the comparisons showed good agreement. Large positive biases in the Z_H and Z_{DR} retrievals during the rain-snow transition period when applying the scattering amplitudes for raindrops disclose the importance of assuming the correct dominant hydrometeor type. The retrievals during the snow period mirrored the changes in hydrometeor habits. Aggregates were associated with small Z_{DR} and large Z_H as expected. An increase in bulk density, as the number of aggregates decreased and that of compact graupel increased, was reflected by a general increase in Z_{DR} and decrease in Z_H. In this case, the use of the size-density relation was important in achieving good agreement between the retrievals and measurements. Two factors that affect measurements of Z_{DR} not considered here but to be explored in future studies, are the importance of particle axis ratios and canting angles.

Reproduction of radar parameters with disdrometer observations is an important initial step in the development of radar-based algorithms for winter precipitation. Well-matched retrievals provide a foundation for reconstructing particle size distributions. Such a capability is required for improving microphysical parameterizations in numerical forecast models and quantifying winter precipitation from radar measurements.

References

Barber, P., and C. Yeh, 1975: Scattering of electromagnetic waves by arbitrarily shaped dielectric bodies. *App. Optics*, **14**, 2864-2872.

Brandes, E. A., G. Zhang, and J. Vivekanandan, 2002: Experiments in rainfall estimation with a polarimetric radar in a subtropical environment. *J. Appl. Meteor.*, **41**, 674-685.

Holroyd, III, E. W., 1971: The meso- and microscale structure of Great Lakes snowstorm bands: A synthesis of ground measurements, radar data, and satellite observations. Ph.D. dissertation, State University of New York at Albany, 148 pp.

Ishimaru, A., 1991: *Electromagnetic Wave Propagation, Radiation, and Scattering*. Prentice Hall, 637 pp.

Kruger, A., and W. F. Krajewski, 2002: Two-dimensional video disdrometer: A description. *J. Atmos. Oceanic Technol.*, **19**, 602-616.

Locatelli, J. D., and P. V. Hobbs, 1974: Fall speeds and masses of solid precipitation particles. *J Geopys. Res.*, 79, 2185-2197.

Ryzhkov, A. V., D. S. Zrnic, and B. A. Gordon, 1998: Polarimetric method for ice water content determination. *J. Appl. Meteor.*, **37**, 125-134.

Zhang, G., J. Vivekanandan, and E. Brandes, 2001: A method for estimating rain rate and drop size distribution from polarimetric radar measurements. *IEEE Trans. Geosci. Remote Sens.*, **39**, 830-841.